SUPPLEMENTARY INFORMATION

SUPPLEMENTARY METHODS

Estimation of the extent of channel block. Patch-clamp current recordings were sampled at 100 kHz, filtered (cascaded cut-off frequency ≅ 30 kHz), and idealized using the hidden-Markov-modeling-based SKM option in QuB software[1]. Single-channel current amplitudes, estimated during the idealization step, were plotted as I-V curves from which the single-channel conductances of main (open, deprotonated) and sub- (open, protonated) levels were estimated as the slopes of linear fits (Fig. 1c of printed version). Fits to sublevel I-V curves often displayed positive *y*-intercepts, which we attribute to some degree of inward rectification introduced by the engineered positive charges. Thus, for the plot in Fig. 1c, the measured I-V curves were voltage-shifted so that they all intersect the *y*-axis at zero pA. This makes the visual comparison of the different slopes much easier. The extent of channel block for each construct in Fig. 1d was calculated as the difference between the conductance-values of the main level and the sublevel, normalized by the conductance of the main level. This calculation was trivial for those constructs displaying current fluctuations between clearly distinct sub- and main levels (triangles in Fig. 1d) but a different approach was needed for those constructs exhibiting only one level of conductance. If the conductance of the single current-level observed was lower than the wild-type's (~84 pS) by a factor between zero and 0.9 (an arbitrary, yet reasonable threshold), then the single conductance-level was assumed to correspond to the protonated form, and the extent of channel block was calculated taking the wild-type's conductance as the main level, and that of the lysine construct in question as the sublevel (circles in Fig. 1d). The δL9'K mutant illustrated in Fig. 3a is an example of this group of mutants. One exception was δGlu -1', in which case the

conductance of the Glu-to-Ala mutant (~67 pS) was taken as the main level so as to subtract the effect of the negative charge. The other exception was δLys 20', in which case the conductance of the wild-type was taken as the sublevel, and that of the Lys-to-Ala mutant as the main level. If, however, the ratio between the conductance of the single current-level and that of the wild-type receptor was larger than 0.9, then an extent-of-channel-block value of zero was assigned (black squares in Fig. 1d). Two exceptions here were δLys 0' (which was compared to the alanine mutant) and δAla 4'. For these two positions, the extent-of-block values plotted in Fig. 1d (red squares) are predictions based on the block-values observed at neighboring locations. This responds to the idea that the failure of lysines at 0' and 4' to induce channel block is due to their highly-acidic pK_as rather than to the lack of blocking effect of positive charges engineered at these two positions (see text). The extent-of-channel-block values corresponding to positions δIle18' and δPro23' were also estimated in a different manner. Lysines engineered at these two positions elicited clear fluctuations of the current between a wild-type-like level and a sublevel of lower conductance (sub-to-main ratio < 0.9) but, because the occupancies of the two open levels were insensitive to changes in pH, these fluctuations are likely to reflect a phenomenon other than the protonation/deprotonation of the lysines. Thus, the extent-of-block values at these two positions were estimated ignoring the occurrence of the sublevel.

Single-channel kinetic analysis. Transition rates were estimated using an interval-based maximum-likelihood approach that includes an approximate solution to the missed-events problem[2]. A consistent time resolution ('dead time') of 25 μs was imposed retrospectively on the idealized series of open and shut intervals. For kinetic modeling, schemes based on that of Fig. 2a were used, with one open-protonated state, one open-deprotonated state, and with the

particular number of shut states varying among mutants, and even among patches expressing the same mutant. Some histidine mutants displayed three (rather than two) open current-levels. In those cases, a third open state (from which transitions to the other two open states and to shut states were allowed) was added to the model used for kinetic modeling. The pH-dependence of the occupancy probabilities of these three levels suggests that the additional open state represents another deprotonated form of the imidazol ring. It is tempting to identify the two 'deprotonated levels' with the two (neutral) tautomers of histidine, $N^{\varepsilon 2}$-H and $N^{\delta 1}$-H, and the single 'protonated level' with the doubly-protonated imidazolium ion. Another possibility, however, is that the two neutral forms of histidine detected in our electrophysiological recordings simply correspond to two particularly stable orientations of the imidazol ring. The different single-channel conductances of the two open-deprotonated levels could be due to the different dipole moments of the two tautomers or conformers. For all the constructs, the Schwarz Criterion[3] was used to select the number of kinetic states in the model.

Calculation of pK_a-values at the single-molecule level. For the calculation of pK_a-values, all that is needed is the deprotonation rate (Open-H^+ → Open), the protonation rate (Open → Open-H^+), and the pH (Fig. 2a). The ratio between the two proton-transfer rates is the single-molecule counterpart of what in a 'many-molecule' experiment would be the ratio between the concentrations of the deprotonated and the protonated forms of the ionizable residue. This ratio multiplied by the concentration of hydronium ions gives the well-known expression for the acid-dissociation equilibrium constant, or K_a, of an acid-base pair. The pK_a-values of the εNH_2 group of lysine and of the guanidine group of arginine in model compounds dissolved in water ('bulk' pK_a-values) are ~10.4 and ~12.0, respectively. In the case of histidine, the individual pK_as of the

$N^{\varepsilon 2}$-H and $N^{\delta 1}$-H tautomers ('microscopic' pK_as) are often combined into a 'macroscopic' pK_a, the value of which is ~6.4 (Ref. 4). It can be easily shown that this 'macroscopic' acid-dissociation equilibrium constant is simply the sum of the two 'microscopic' equilibrium constants. For the subset of histidine mutants that displayed two 'open-deprotonated' current levels, the proton-transfer rates and pK_as reported in Fig. 2b, c and Table 1 were *calculated* from the proton-transfer rates *measured* for each individual open-deprotonated state. Thus, these values can also be considered 'macroscopic', and correspond to those one would have measured if the existence of the two distinct deprotonated forms of the histidine had gone undetected.

Model representation. In Fig. 2c, the estimated ΔpK_a-values were mapped onto a representation of the 0' – 17' δM2 stretch using the atomic coordinates in the 1OED PDB file[5], a model of the transmembrane portion of the *Torpedo* (a muscle-type) AChR in the closed state. It should be noted, however, that the rotational angle of δM2 inferred from our *open*-state data is not identical to that proposed by Unwin's *closed*-state model. For example, our data places position 14' farther from the center of the pore, and 16' closer to it. It would seem natural to ascribe this difference to the closed ⇌ open conformational rearrangement but the small rotation (~20º) that is needed to superimpose both data has the opposite direction to that proposed by Unwin to underlie gating[5]. Rather, we prefer to emphasize that the difference in helix rotation between the two models is small, and that the details of Unwin's closed-channel model should be taken as tentative due to the limited resolution of the electron-density map, and to the fact that the experimental data the model is based on (i.e., affinity labeling, functional studies of mutants, cysteine modification) do not point univocally to a specific rotational angle.

SUPPLEMENTARY DISCUSSION

A small water-filled cavity lined by 15'. The 15' position displays some unique properties. A protonated lysine at this position exerts a relatively minor effect on the current (extent of channel block ≅ 0.25; Fig. 1d), implying a location on the 'back' of the α-helix, away from the aqueous lumen. On the other hand, however, the pK_a of the lysine's εNH_2 group engineered at this position is high (deprotonation of this group was only evident in recordings performed at pH = 9.0), which suggests a polar microenvironment. Together, these two apparently contradictory observations would be consistent with the existence of a well-delimited water-filled pocket, continuous with the extracellular solution, in this region of the open channel. The electrostatic properties of this putative small cavity differ, however, from those of the central aqueous lumen. The '15'-cavity' slightly destabilizes ($\Delta pK_a \cong -0.73$), whereas the central pore stabilizes ($0 < \Delta pK_a < +2.00$), the positively-charged form of engineered histidines relative to bulk water (Supplementary Fig. 2). Probably, this difference simply reflects a lower water content, and hence a reduced water polarizability, for the cavity lined by 15' (Ref. 6). The existence of such small cavities or crevices near the AChR's 15' position would not be entirely surprising since the 15' positions of the anion-selective $GABA_A$ and glycine receptors have been proposed to line small 'pockets' where *n*-alcohols and anesthetics bind with state-dependent affinities[7,8]. It is not clear whether these molecules can bind to similar cavities in muscle-type AChRs[9], and modulate gating, but it is interesting to note the extent to which structural details are conserved throughout this superfamily of receptor-channels.

Rotation or a change in tilt angle? On the basis of the open-channel data in Figs 1d and 2b, c, and the results from photoaffinity labeling of the closed-channel pore[9,10], it seems inescapable to conclude that it is mainly the tilt angle of M2 that changes upon opening to bring about the presumed expansion of the pore. However, on the basis of a comparison between cryo-electron microscopy images in the closed and open states, Unwin proposed that the M2 helices *rotate* during gating[11]. The latest version of this model[5] suggests a rotation of only 15º, which is certainly too small to be detected as changes in the pore lining, especially since the rotational angle of M2 in the closed state is not known with enough precision[12]. In any case, it is clear that, with or without rotation, the gating conformational change does not involve the alternative exposure of different faces of the M2 α-helices to the lumen; small rearrangements like these may be necessary to ensure fast gating kinetics during synaptic transmission. This notion, though, seems irreconcilable with gating models based largely on the results of disulfide-trapping experiments in $GABA_A$ receptors (a member of the Cys-loop receptor superfamily), which posit that a much larger rotation (~100º) of the M2 helices underlies the closed ⇌ open conformational change[13,14]. In our opinion, these results do not necessarily indicate that such markedly rotated M2 helices are representative of the average open-channel structure. Rather, the pronounced rotation (which would be needed to bring pairs of cysteines in close proximity) might simply represent an orientation occupied with very low probability from which disulfide-bond formation proceeds extremely fast.

Protonation state of naturally-occurring ionizable residues. The 0' position, occupied by a basic residue in all Cys-loop receptors (both cation- and anion-selective; Fig. 1a), appears to be pointing away from the AChR's pore's lumen (Fig. 1d), and to be either deprotonated (Fig. 2 and

Table 1) or charged but highly screened by its microenvironment. This situation is consistent with that of a basic residue located near the narrowest constriction of a cation-selective channel. In stark contrast, however, on the basis of the effect of mutations on the anion-*versus*-cation selectivity of glycine receptors, this position (an arginine) has been suggested to be protonated, to face the channel's lumen directly, and to represent the main determinant of charge selectivity in this anion-selective Cys-loop receptor[15]. It is interesting to think of a role for the proline residue present in the M1-M2 loop of some of the anion-selective subunits, only two residues away from the 0' position, in this putative drastic reorientation of side chains. The 4' position, occupied by lysine in both subunits of the cation-selective serotonin ionotropic receptor (5-HT_{3A} and 5-HT_{3B}; Fig. 1a), exhibits very similar properties to 0' (Figs 1d and 2b, c, and Table 1), and thus we predict that this lysine might also be completely deprotonated; this offers an alternative explanation to the lack of effect of mutations of this residue on the single-channel conductance of 5-HT_{3A} homomers[16]. The 15' position of the 5-HT_{3B} subunit is occupied by an arginine, and it follows from our data that this residue should be protonated at physiological pH (Table 1), although exerting only a small blocking effect on the current (Fig. 1d). The 17' position of $GABA_A$ β-type subunits is occupied by a histidine, which, with a pK_a ≅ 6.4 (Table 1), is expected to be predominantly deprotonated at pH = 7.4 (imidazole/imidazolium$^+$ ≅ 10). This prediction, however, must be taken as tentative because the possible effect of the permeating ions (anions in the $GABA_A$ receptor, cations in the AChR) on the side-chain's pK_a should not be overlooked. Finally, the protonation state of the glutamates in the -1' EEEEQ ring of the muscle AChR (Fig. 1a), an essential component of the AChR's selectivity filter[17], is more difficult to predict on the basis of our results. Although it is evident that these residues carry some negative charge [the Glu-to-Ala mutation in the δ subunit decreased the conductance from (84 ± 0.5) pS

to (67 ± 0.9) pS, for example], the extent to which the repulsive charge-charge interactions among the glutamates increase their proton affinities is hard to ascertain using a histidine as a probe (Table 1). It is clear that further experiments and additional electrostatic calculations are needed before a precise net charge for the AChR's -1' ring can be suggested. Important steps toward this goal have already been taken[18,19].

REFERENCES

1. Qin, F. Restoration of single-channel currents using the segmental k-means method based on hidden Markov modeling. *Biophys. J.* **86**, 1488-1501 (2004).

2. Qin, F., Auerbach, A. & Sachs, F. Estimating single-channel kinetic parameters from idealized patch-clamp data containing missed events. *Biophys. J.* **70**, 264-280 (1996).

3. Schwarz, G. Estimating the dimension of a model. *Ann. Statist.* **6**, 461-464 (1978).

4. Tanokura, M. ^{1}H-NMR study on the tautomerism of the imidazole ring of histidine residues I. Microscopic p*K* values and molar ratios of tautomers in histidine-containing peptides. *Biochim. Biophys. Acta* **742**, 576-585 (1983).

5. Miyazawa, A., Fujiyoshi, Y. & Unwin, N. Structure and gating mechanism of the acetylcholine receptor pore. *Nature* **423**, 949-955 (2003).

6. Brandsburg-Zabary, S., Fried, O., Marantz, Y., Nachliel, E. & Gutman, M. Biophysical aspects of intra-protein proton transfer. *Biochim. Biophys. Acta* **1458**, 120-134 (2000).

7. Williams, D. B. & Akabas, M. H. γ-aminobutyric acid increases the water accessibility of M3 membrane-spanning segment residues in γ-aminobutyric acid type A receptors. *Biophys. J.* **77**, 2563-2574 (1999).

8. Mascia, M. P., Trudell, J. R. & Harris, R. A. Specific binding sites for alcohols and anesthetics on ligand-gated ion channels. *Proc. Natl. Acad. Sci. U. S. A.* **97**, 9305-9310 (2000).

9. Arévalo, E., Chiara, D. C., Forman, S. A., Cohen, J. B. & Miller, K. W. Gating-enhanced accessibility of hydrophobic sites within the transmembrane region of the nicotinic acetylcholine receptor's δ subunit. A time-resolved photolabeling study. *J. Biol. Chem*. **280**, 13631-13640 (2005).

10. White, B. H. & Cohen, J. B. Agonist-induced changes in the structure of the acetylcholine receptor M2 regions revealed by photoincorporation of an uncharged nicotinic noncompetitive antagonist. *J. Biol. Chem.* **267**, 15770-15783 (1992).

11. Unwin, N. Acetylcholine receptor channel imaged in the open state. *Nature* **373**, 37-43 (1995).

12. Kim, S., Chamberlain, A. K. & Bowie, J. U. A model of the closed form of the nicotinic acetylcholine receptor M2 channel pore. *Biophys. J.* **87**, 792-799 (2004).

13. Horenstein, J., Wagner, D. A., Czajkowski, C. & Akabas, M. H. Protein mobility and GABA-induced conformational changes in $GABA_A$ receptor pore-lining M2 segment. *Nature Neurosci.* **4**, 477-485 (2001).

14. Goren, E. N., Reeves, D. C. & Akabas, M. H. Loose protein packing around the extracellular half of the $GABA_A$ receptor β_1 subunit M2 channel-lining segment. *J. Biol. Chem.* **279**, 11198-11205 (2004).

15. Keramidas, A., Moorhouse, A. J., Pierce, K. D., Schofield, P. R. & Barry, P. H. Cation-selective mutations in the M2 domain of the inhibitory glycine receptor channel reveal determinants of ion-charge selectivity. *J. Gen. Physiol.* **119**, 393-410 (2002).

16. Gunthorpe, M. J., Peters, J. A., Gill, C. H., Lambert, J. J. & Lummis, S. C. R. The 4' lysine in the putative channel lining domain affects desensitization but not the single-channel conductance of recombinant homomeric 5-HT_{3A} receptors. *J. Physiol. (London)* **522.2**, 187-198 (2000).

17. Corringer, P. J. *et al.* Mutational analysis of the charge selectivity filter of the α7 nicotinic acetylcholine receptor. *Neuron* **22**, 831-843 (1999).

18. Adcock, C., Smith, G. R. & Sansom, M. S. P. Electrostatics and the ion selectivity of ligand-gated channels. *Biophys. J.* **75**, 1211-1222 (1988).

19. Wilson, G. G., Pascual, J. M., Brooijmans, N., Murray, D. & Karlin, A. The intrinsic electrostatic potential and the intermediate ring of charge in the acetylcholine receptor channel. *J. Gen. Physiol.* **115**, 93-106 (2000).

20. Humphrey, W., Dalke, A. & Schulten, K. VMD: visual molecular dynamics. *J. Molec. Graphics* **14**, 33-38 (1996).

21. Imoto, K. *et al*. Rings of negatively charged amino acids determine the acetylcholine receptor channel conductance. *Nature* **335**, 645-648 (1988).

SUPPLEMENTARY FIGURE LEGENDS

Supplementary Figure 1. General properties of the AChR. a, Membrane-threading pattern common to all Cys-loop receptors, a superfamily of neurotransmitter-gated ion channels which, in vertebrates, includes receptors to ACh, serotonin, GABA, and glycine. The approximate locations of the 1' and 19' residues on the pore-lining M2 segment (Fig. 1a) are noted. The portion of the δ subunit studied in this paper is sketched in red. **b,** Ribbon representation of the 1OED PDB file[5], a model of the transmembrane portion of *Torpedo*'s electric-organ AChR (a muscle-type AChR) in the closed state, as viewed from the extracellular side. Pore-lining M2 segments are colored black. M1, M3, and M4 segments are colored orange. M1, M3, and M4 shield M2 from membrane phospholipids[5]. In adult muscle, the γ subunit is replaced by the ε subunit. The molecular image was made with VMD[20]. **c,** Effect of pH on the single-channel conductance of the wild-type adult mouse-muscle AChR. The protonation/deprotonation of naturally-occurring ionizable residues was not resolved as discrete current fluctuations at any of the pH-values tested. The number of independent patches analyzed was: 3 at pH = 5.0; 10 at pH = 6.0; 24 at pH = 7.4; 8 at pH = 9.0; and 6 at pH = 10.5. Vertical error bars (standard errors) are smaller than the experimental points.

Supplementary Figure 2. pK_a-shifts along M2. The ΔpK_a-values in Table 1 are plotted against residue number. Downshifted pK_a-values reflect the uncompensated loss of solvation free-energy, which is greatest in the 'back' of the α-helix. Upshifted values, observed at pore-lining positions, very likely reflect the positive-charge stabilizing effect of the -1' ring of glutamates[19,21] (Fig. 1a). Note that the upshift is much smaller in magnitude than the downshift. The solid line is a cubic-spline interpolation. The thick vertical line emphasizes the zero ΔpK_a.

The top *x*-axis indicates the ΔGº associated with the transfer of the protonated form of the ionizable residue (AH^+) from bulk water to its particular position in the protein relative to the corresponding ΔGº for the deprotonated form (A). Horizontal error bars (standard errors) are smaller than the experimental points. The pore's lumen is to the right of the plot.

Supplementary Figure 3. Kinetic characterization of proton-transfer reactions. a, b, Dwell-time histograms of the protonated (**a**) and deprotonated (**b**) open levels of the δL9'H mutant (Fig. 3b) corresponding to one representative recording at pH = 7.4 (316,245 intervals). **c**, **d,** Dwell-time histograms of the protonated (**c**) and deprotonated (**d**) open levels of the δS12'K mutant (Fig. 3c) corresponding to one representative recording at pH = 7.4 (58,450 intervals). Shut-time histograms are not shown. Solid lines are monoexponential densities computed from the estimates of transition rates with allowance for missed events (time resolution = 25 μs). Transition rates were estimated from maximum-likelihood fitting of dwell-time series to kinetic models based on that of Fig. 2a. The insets show the relevant portion of such model, and the thick arrows indicate the transition rates that determine the duration of open-protonated or open-deprotonated intervals.

SUPPLEMENTARY FIGURES

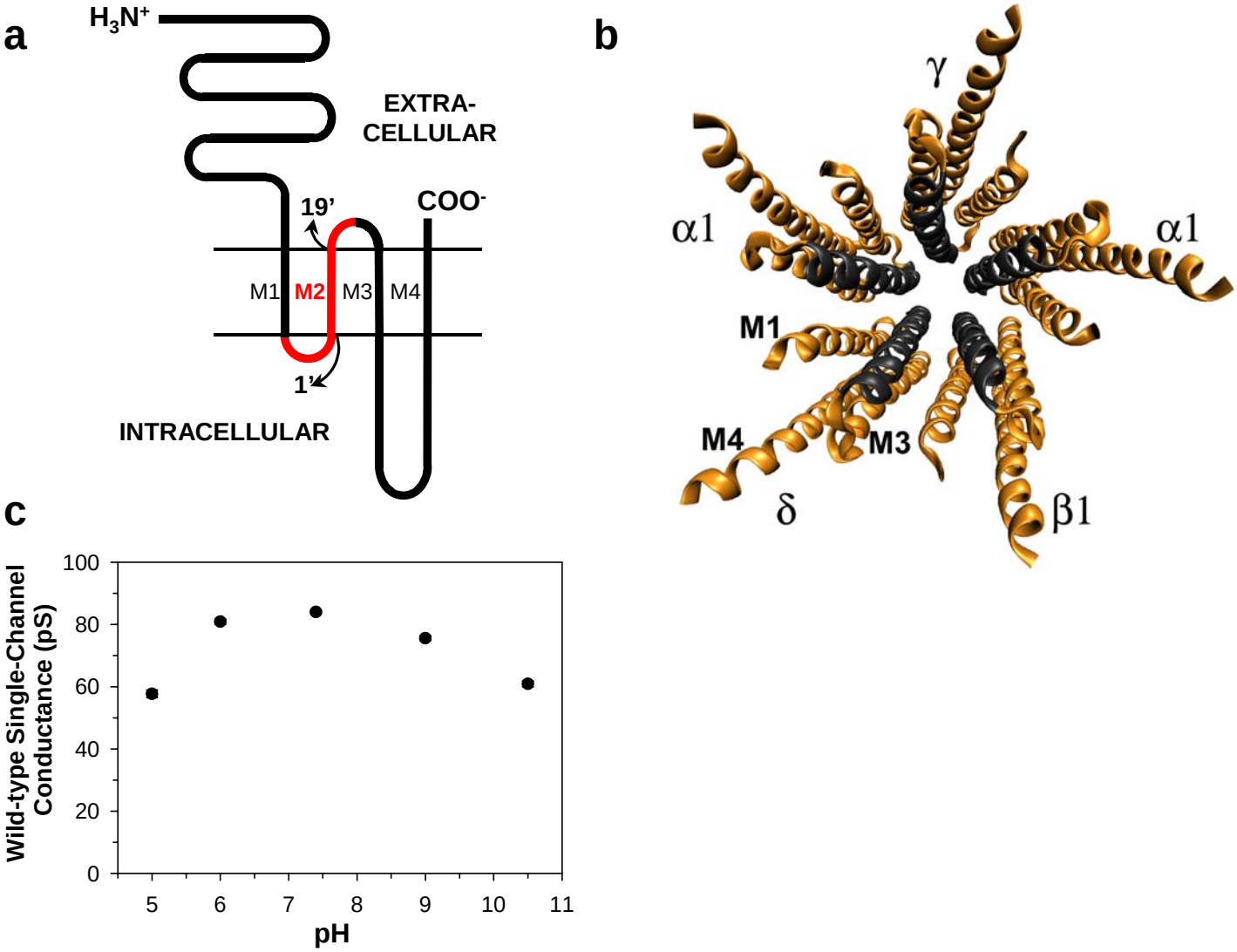

Supplementary Figure 1

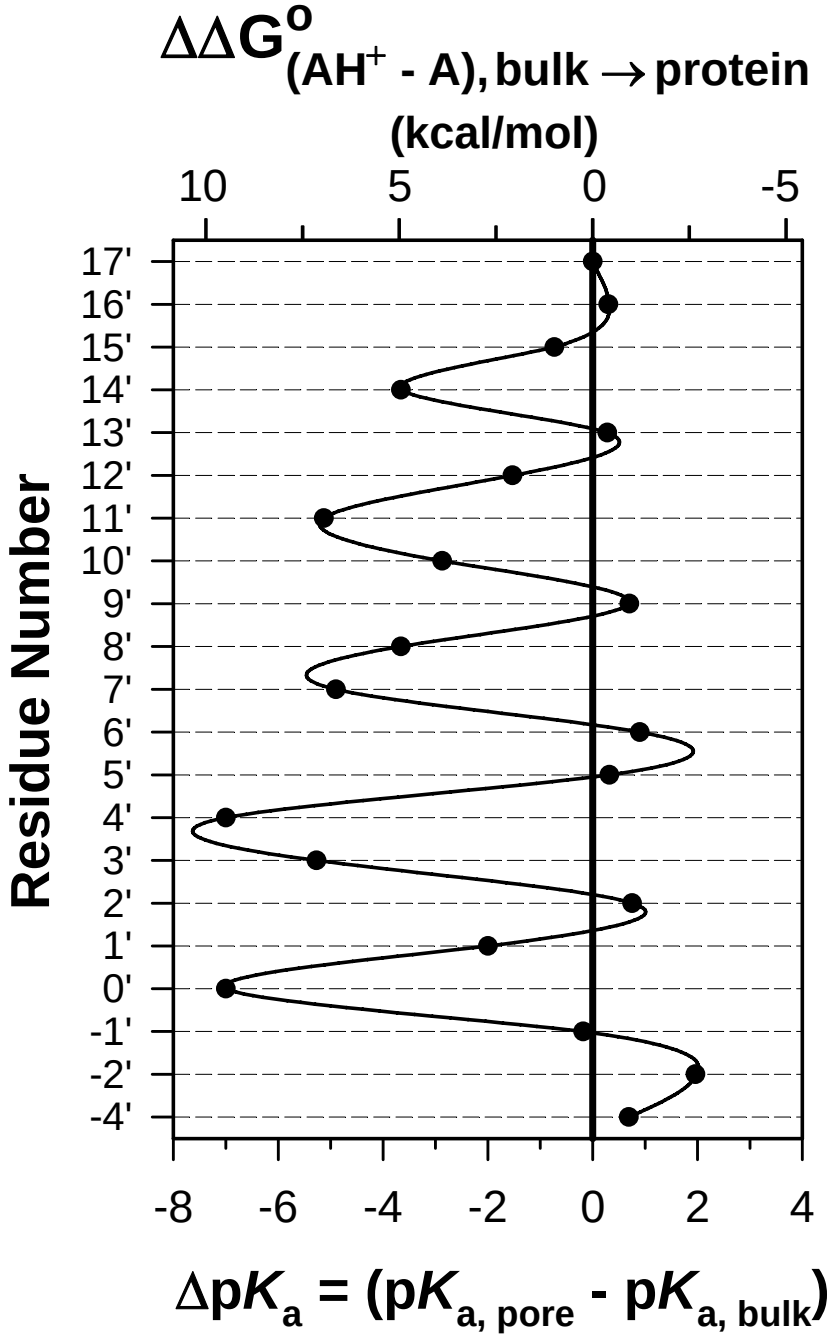

Supplementary Figure 2

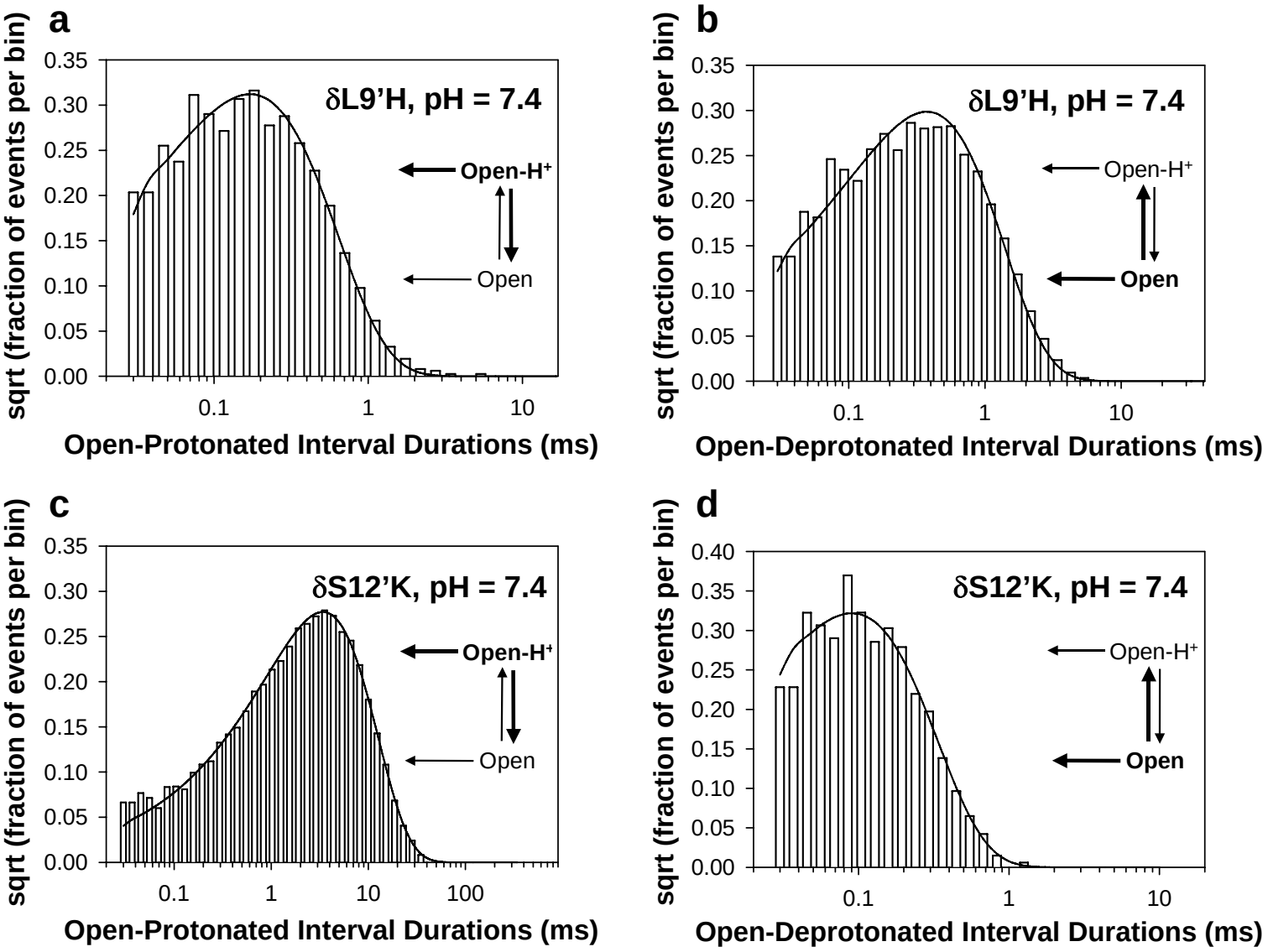

Supplementary Figure 3